minerals

MDPI

Article

Effect of Chemical Corrosion and Axial Compression on the Dynamic Strength Degradation Characteristics of White Sandstone under Cyclic Impact

Jinchun Xue [1], Zhuyu Zhao [1], Longjun Dong [2,*], Jiefang Jin [3], Yingbin Zhang [1], Li Tan [1], Ruoyan Cai [1] and Yihan Zhang [2]

[1] School of Energy and Mechanical Engineering, Jiangxi University of Science and Technology, Nanchang 330013, China; xuejinchun@jxust.edu.cn (J.X.); zhuyuzhao@njfu.edu.cn (Z.Z.); zhangyingbin@jxust.edu.cn (Y.Z.); 20210280854000003@ecjtu.edu.cn (L.T.); exampie19951123@163.com (R.C.)
[2] School of Resources and Safety Engineering, Central South University, Changsha 410083, China; zyh6324@csu.edu.cn
[3] Jiangxi Provincial Key Laboratory of Environmental Geotechnology and Engineering Disaster Control, Jiangxi University of Science and Technology, Ganzhou 341000, China; jjf_chang@126.com
* Correspondence: lj.dong@csu.edu.cn

Abstract: Both chemical corrosion and axial compression impose critical influences on the internal microstructure of rock. Meanwhile, chemical corrosion can change a rock's mineral composition, which in turn affects the physical and mechanical properties of the rock. To investigate the dynamic strength characteristics of white sandstone under the coupling effect of axial load and chemical corrosion, a dynamic and static combined loading test device was adopted for performing cyclic impact tests on white sandstone immersed in chemical solution. The results show that with the increasing number of cycles under the same load, the peak strength of the rock presented a trend of 'strengthening first and then weakening'. The strength of rock resistance to impact failure reached its maximum when the solution of pH was 7 and axial pressure was 12.6 MPa. Under the same axial pressure, the effect of solution pH on the initial dynamic strength of white sandstone is a normal distribution. Acidic and alkaline environments are harmful to rocks during the initial impact, while neutral environments exert little effect and the pH of the solution influences the particle size of impact crushing particles. In addition, the chemical solution has a significant effect on the deterioration of rock strength during the process of initial impact, and the effect is inconspicuous in the later period.

Keywords: rock mechanics; cyclic impact; chemical corrosion; axial compression; strength degradation

Citation: Xue, J.; Zhao, Z.; Dong, L.; Jin, J.; Zhang, Y.; Tan, L.; Cai, R.; Zhang, Y. Effect of Chemical Corrosion and Axial Compression on the Dynamic Strength Degradation Characteristics of White Sandstone under Cyclic Impact. *Minerals* **2022**, *12*, 429. https://doi.org/10.3390/min12040429

Academic Editor: Gianvito Scaringi

Received: 3 March 2022
Accepted: 29 March 2022
Published: 31 March 2022

1. Introduction

Certain large-scale infrastructure construction and mining projects are inseparable from geotechnical engineering. These include projects such as large-section tunnel excavation [1], resource exploitation [2,3], subgrade blasting [4], directional damming and interception projects [5,6]. The rock not only bears the static stress of structure during construction but also experiences the erosion of the chemical environment for a long time. In the process of blasting excavation, the stability of rock is inevitably influenced by frequent drilling and blasting vibrations [7]. The coupling of force and chemical corrosion has a critical influence on the stability of engineering rock mass in the long term [8].

Over the last decades, many scholars have performed a lot of research on investigating rock dynamic mechanical properties under various conditions. Li et al. [9] conducted a uniaxial cyclic impact compression test on granite through an improved split Hopkinson pressure bar (SHPB). The results show that the damage accumulation of the rock increased with the number of cyclic impacts. Gong et al. [10] carried out a one-dimensional experimental study on the dynamic characteristics of rock under combined dynamic and

static loading, revealing that the impact strength is maximally strengthened with an axial compression ratio of 0.6~0.7. Zhou et al. [11] studied the dynamic mechanical behavior and failure characteristics of mudstone using the split Hopkinson pressure bar test device, and proposed a criterion for the dynamic strength of mudstone. Jin et al. [12] discussed the effects of different static loads on the failure pattern of rock subjected to cyclic impact and concluded that rock with an axial static load had extremity effects in the process of destruction. Ding et al. [13] investigated the failure process and the mechanical properties of limestone under different chemical solutions, finding that the strength of limestone decreased due to the chemical solutions. Xie et al. [14] conducted in situ stress restoration tests on cores of different burial depths and obtained rock behaviors under the action of in-situ stress, temperature, and pore pressure. Siddiqua et al. [15] explored the saturated mechanical behavior of light backfill and dense backfill, which clarified the strengthening effect of pore fluid chemistry on shear strength, stiffness, and yield behavior. Han et al. [16] compared microstructure, deformation characteristics, and the mechanical behavior of rock by chemical solutions with different pH, different concentrations, and different compositions, revealing that rock had a conversion trend of brittle to ductile after chemical corrosion. Xia et al. [17] conducted the whole process of compression failure of multi-crack limestone and limestone under different chemical solutions by adopting a self-developed micro loading instrument, which obtained the deformation characteristics of rock specimens, the mode of crack initiation, propagation and penetration as well as the different overlapping modes of rock bridges when they were damaged. Li et al. [18] studied the main components of calcareous cemented feldspar rock under different pH, and a rock damage model that could be applied to acidic solutions was put forward. Through scanning electron microscope (SEM) and X-ray diffraction (XRD) technology, Cui et al. [19] analyzed the mechanical and corrosion damage of the surface and mineral components of rock after the action of 0.01 mol/L NaOH solution with a pH of 12 and revealed internal changes in the rock under that solution.

Scholars both at home and abroad have conducted in-depth studies on the mechanical properties of rocks in static or quasi-static conditions [20–24]. Currently, studies on the mechanical properties of rock have mainly focused on a single factor, such as axial static load [25], impact load [26], and chemical corrosion [27]. However, there is less investigation on the rock cyclic impact failure and damage accumulation under the coupling of axial pressure and chemical corrosion. Based on split Hopkinson pressure bar (SHPB) test technology combined with one-dimensional stress wave theory, cyclic impact experiments were carried out on white sandstone immersed in chemical solutions with different pH and axial pressures, which explored fatigue damage mechanism and the characteristics of strength weakening of white sandstone under multi-factor coupling. The mechanism of strength and fatigue failure also provides a theoretical basis for the safe and effective construction management of blasting engineering under complex geological conditions.

2. Experimental Method

2.1. Rock Preparation

The rock material used in the present study was white sandstone that was taken from Kunming, Yunnan, China. These rock blocks are off-white, with good integrity and homogeneity as the research objects. Sandstone samples were subjected to professional elemental analysis and mineral identification, as shown in Figure 1. They were composed primarily of quartz, feldspar (e.g., potassium feldspar, sodium feldspar, and calcium feldspar), clay, calcite and a small number of hematite, quick lime and other minerals. The sandstone's quartz was identified as SiO_2. Feldspar was identified as a collection of $KAlSi_3O_8$, $NaAlSi_3O_8$ and $CaAl_2Si_3O_8$. Clay was identified as $xAl_3O_2{\cdot}ySiO_2$. The main component of calcite is calcium carbonate. Furthermore, hematite and quick lime are Fe_2O_3 and CaO, respectively.

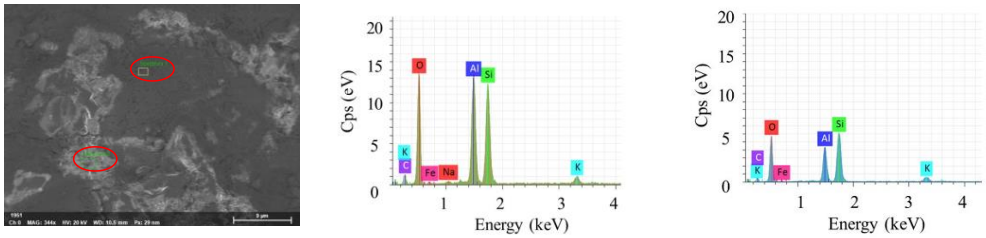

(**a**) (**b**) (**c**)

Figure 1. EDS analysis results. (**a**) EDS sampling point; (**b**) Element at point 1; (**c**) Element at point 2.

According to the size and accuracy requirements of the relevant guidelines of ISRM [28], the size of cylindrical white sandstone specimens is Φ50 mm × 50 mm, and that of unevenness and verticality are less than 0.05 mm by means of carefully grinding both ends of the rock specimens. The processed rock specimens are displayed in Figure 2. The rock specimens were dried and evacuated for 8 h, divided into eight groups, and sealed immersed in the chemical solutions presented in Table 1 for 240 days.

Figure 2. White sandstone specimens (**a**–**c**).

Table 1. Chemical solution.

Composition	Concentration (mol/L)	pH
NaCl	0.1	2, 7, 9, 12
Na_2SO_4	0.1	2, 7, 9, 12

2.2. Experimental Apparatus

In this study, based on the split Hopkinson pressure bar (SHPB) system established previously [29], an experiment system of SHPB is shown in Figure 3, using the laboratory dynamic cyclic impact compression experiment that was performed. The experiment facilities are mainly composed of a dynamic loading system (gas gun, launch cavity and shaped puncher), a test system (CS-1D strain instrument, DL-750 oscilloscope, and laser speedometer), a delivery system and an axial compression system. The delivery system mainly includes an incident bar, transmission bar, and buffer bar, the lengths of which are 2000 mm, 1500 mm, and 500 mm, respectively. All of the elastic bars were made of high-strength 40 Cr alloy steel, a wave velocity of 5400 m/s, a density of 7.81 g/cm^3, and a wave impedance of 4.2 × 10^7 MPa. The special-shaped punch is applied to eliminate PC oscillation and realize half-sine wave loading with constant strain rate loading [30–32].

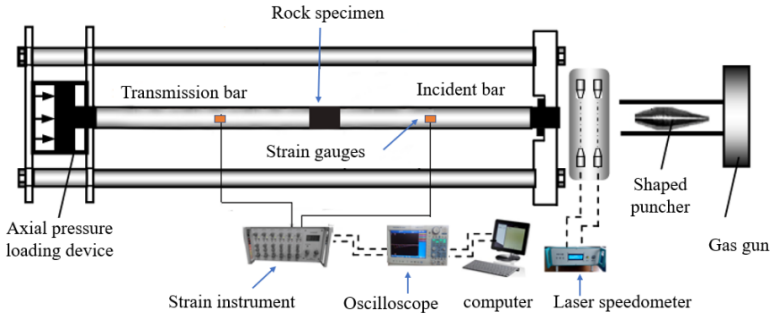

Figure 3. Split Hopkinson pressure bar (SHPB).

2.3. Experimental Method

Before conducting the cyclic impact test, a physico-mechanical parameters test was carried out on the white sandstone specimens by adopting the RMT-150 electro-hydraulic servo control material testing machine. The results of this test are shown in Table 2.

Table 2. Physico-mechanical parameters of white sandstone specimens.

Specimens	Density ($kg \cdot m^{-3}$)	Loading Rate ($MPa \cdot s^{-1}$)	Strain Rate (s^{-1})	Uniaxial Compression Strength (MPa)	Secant Modulus (GPa)	Poisson Coefficient
White sandstone	2321	0.23	1.00×10^{-5}	31.5	17.65	0.25

In order to ensure that cyclic impact test on the white sandstone with the chemical corrosion and axial pressure could be carried out successfully, the experimental method was designed as follows. Four solutions of pH at 2, 7, 9, and 12 were designed. According to the research conducted by Sun et al. [33], in the process of cyclic impact, rock specimens did not show the palpable end effect failure mode when there was no static load. Combined with the value of uniaxial compressive strength test, axial compression was set to four levels of uniaxial compressive strength of 20%, 40%, 65%, 85%, which were respectively 6.3 MPa, 12. 6 MPa, 20.5 MPa and 26.8 MPa. In addition, due to the existence of a threshold value in the cyclic impact load experiment [34], multiple pre-impact tests were required to determine the fixed air pressure in the high-pressure gas chamber of 0.8 MPa. The impact speed of the punch was 4.5 m/s.

The following conditions must be satisfied during the test process:

(1) The incident bar, transmission bar and buffer bar should be kept level.
(2) The magnitude of the axial load should be equal to the axial load value set in advance.
(3) To fix the impact load, it is necessary to strictly ensure that the pressure in the high-pressure air chamber is equal to the value set before each impact, and that the position of the punch in the launching chamber remains unchanged.
(4) The white sandstone specimens were sandwiched between the incident bar and the transmission bar, with petroleum jelly coated on both ends of the specimen to ensure good contact.

3. Typical Stress–Strain Curve during Cyclic Impact

Using a split Hopkinson pressure bar (SHPB), Jin et al. [35]. conducted a series of cyclic impact loading tests on sandstone under different static loading conditions, obtaining a typical dynamic stress–strain curve of sandstone during cyclic impact. The results of the experiments reveal that the sandstone's dynamic strength and the characteristics of deformation were affected by axial compression and the number of cycles. In this study, the cyclic impact test of white sandstone soaked in NaCl with pH of 9 and axial pressure of 6.3 MPa was taken as an example for analyzing the different stages of the test. Figure 4 presents an overlay chart of the typical waveform recorded during the cycle impact test. It can be observed from the figure that the amplitude of the incident wave has not changed significantly and that the superposition of waveform basically coincides, achieving the requirements of the constant-amplitude cyclic impact test. The reflected wave amplitude of the specimen increases and the transmitted wave amplitude decreases gradually with the increasing number of impacts, and the change of cyclic impact is obvious in the middle and later periods. This phenomenon occurs regardless of axial compression and pH. Since the size of the white sandstone specimen tested is small, the homogeneity hypothesis is introduced, satisfying the expression $\varepsilon_l(t) + \varepsilon_r(t) = \varepsilon_t(t)$ [36]. According to one-dimensional stress wave theory, the collected voltage signal is processed. Stress, strain, and average strain rate can be calculated using the following formula.

$$\sigma_s = \frac{A_e E_e}{2A_s}(\varepsilon_l + \varepsilon_R + \varepsilon_T) \quad (1)$$

$$\varepsilon_S = -\frac{C_e}{L_s}\int_0^l (\varepsilon_l - \varepsilon_R - \varepsilon_T)dt \quad (2)$$

$$\dot{\varepsilon_s} = \frac{C_e}{L_s}(\varepsilon_l - \varepsilon_R - \varepsilon_T) \quad (3)$$

In these Equations, *As* and *Ls* are the cross-sectional area and length of the specimen, respectively; *Ae*, *Ee* and *Ce* represent elastic rod cross-sectional area, elastic modulus and longitudinal wave velocity, respectively; ε_l, ε_R and ε_T denote the incident, reflection and transmission wave signals, respectively.

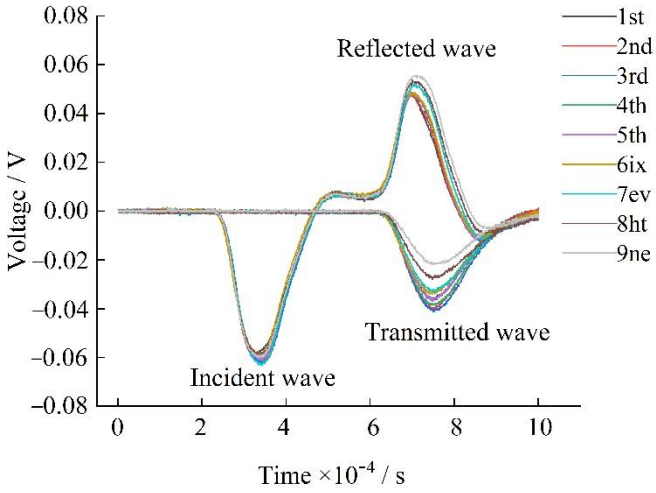

Figure 4. Typical stress waves during cyclic impact.

The typical stress–strain curves of the white sandstone under cyclic impact loading tests are shown in Figure 5. It can be observed from the figure that the stress–strain curve of the whole cyclic impact test can be divided into three types. The initial stress–strain curve (one to five impacts) is a semi-elliptic high flat curve. In addition, the elastic modulus, peak stress, and maximum strain have not changed significantly. The stress in the loading stage increases sharply with the increase of strain. The slope is steep, and the elastic modulus value is large. The maximum stress at this stage represents the maximum impact stress value that the specimen can withstand during the entire impact process, which is called the peak strength. However, the stress in the unloading stage drops sharply with the increasing strain.

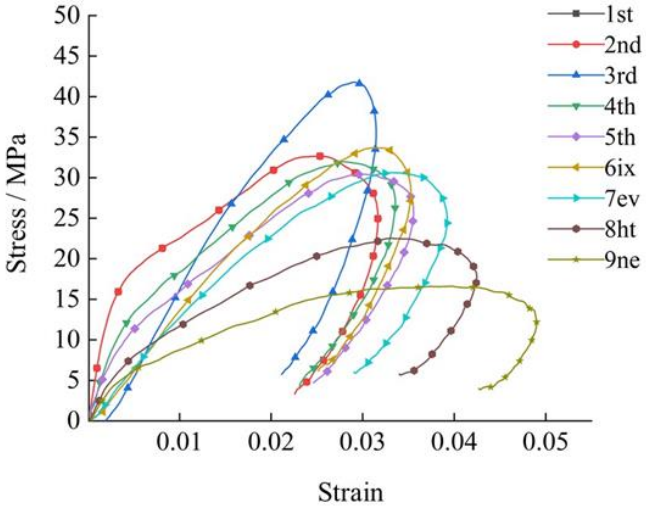

Figure 5. Typical stress-strain curve during cyclic impact.

In the mid-term (sixth to eighth impacts), there exists a gradient parabola. The changes in elastic modulus, peak stress, and maximum strain are more prominent than those in the initial stage. Besides, the change of stress with strain is larger than that of the initial stage in the loading section and unloading section. It shows that the micro-cracks in white sandstone are compacted and closed, resulting in small changes in modulus. Owing to the medium-term impact load, pore cracks begin to gradually expand and penetrate, and the bearing capacity suddenly decreases.

The later stage (the ninth impact) is a low flat parabolic curve, the peak stress is small, and the strain at the tail of the curve tends to decrease, which is consistent with the research results of the rock impact failure test under the one-dimensional dynamic and static combination determined by the literature [22]. This demonstrates that the white sandstone has not been completely destroyed and still possesses a certain load-bearing capacity, though it's capacity is weak. Therefore, it cannot be loaded under the same axial compression conditions.

4. Experimental Results and Discussion

This study lists the physical parameters and test data of a representative set of specimens, as listed in Table 3.

Table 3. Parameters of some specimens and the number of cyclic impacts.

σ_{as} (MPa)	Numbering	L (mm)	D (mm)	ρ (kg·cm^{-3})	pH	σ_{fd} (MPa)	σ_{md} (MPa)	σ_{cs} (MPa)	The Number of Cycle Impact
6.3	w-062	47.03	49.08	2315	2	39.64	43.51	49.81	7
	w-052	47.05	49.09	2329	7	43.12	43.20	49.50	9
	w-033	47.06	49.11	2312	9	42.68	42.68	48.98	8
	w-042	47.06	49.09	2322	12	42.03	49.43	55.73	7
12.6	w-063	47.05	49.12	2327	2	37.16	41.42	54.02	5
	w-053	47.06	49.09	2312	7	51.56	51.56	64.16	8
	w-034	47.05	49.09	2322	9	49.61	49.61	62.21	6
	w-043	47.07	49.10	2328	12	39.87	50.10	62.70	5
20.5	w-064	47.06	49.14	2312	2	38.46	38.46	58.96	4
	w-054	47.08	49.13	2329	7	43.11	43.11	63.61	5
	w-037	47.05	49.10	2329	9	40.72	40.72	61.22	5
	w-044	47.05	49.04	2320	12	40.75	42.83	63.33	2
26.8	w-065	47.06	49.12	2308	2	27.26	31.92	58.72	2
	w-055	47.06	49.05	2329	7	32.01	32.01	58.81	3
	w-036	47.06	49.06	2318	9	28.82	30.51	57.31	3
	w-045	47.07	49.02	2317	12	25.71	29.98	56.78	2

Note: σ_{as} is the axial pressure, ρ is density, σ_{fd} is initial impact stress peak, σ_{md} is the maximum stress peak of the cyclic impact, and σ_{cs} is the combined static–dynamic strength.

4.1. The Trend of Cyclic Impact Number

Figure 6 shows the relationship between the pH of the solution, the axial pressure, and the number of cyclic shocks. The number of cyclic impacts decreases with the increase of the axial pressure, and the number of impacts that can be endured under the axial pressure of 6.3 MPa is the most. As shown in the analysis, when the axial pressure is within a certain lower limit range, with the same load repeatedly repeating the impact, the original void inside the specimens will be closed first, and the ability and frequency of the sample to resist impact will be accordingly enhanced [37]. However, when the axial pressure is within a certain higher limit range, the secondary microcracks grow into pore cracks that penetrate the entire cross-section. During this process, the damage expands and the ability of the

sample to resist external damage decreases sharply. In the middle and later stages of the impact stages, the whole rock specimen is finally damaged by tensile shear. Furthermore, this is similar to the dynamic characteristics of the cumulative damage evolution during excavation of underground jointed rock under repeated seismic load that is mentioned in Ref. [38]. With the pH of the solution, the number of shocks is normally distributed. The pH of the solution deviates from neutral, which indicates that the lower the number of shocks, the more obvious the corrosion effect of the solution.

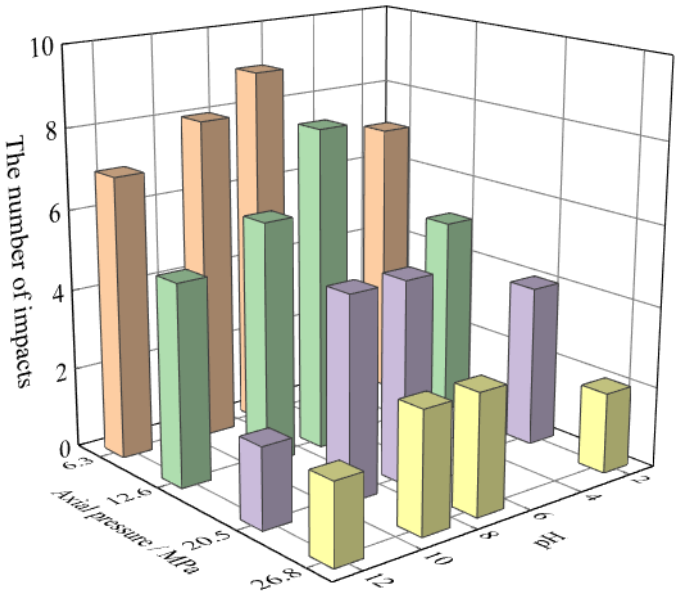

Figure 6. The trend of cyclic impact number.

4.2. Relationship between Initial Peak Stress and Axial Pressure

The peak strength of the rock represents the maximum stress caused by the impact resistance of the white sandstone specimens during impact. The strength of the specimen gradually weakens when the number of cyclic impacts increases. Although the overall peak deterioration law is similar, there also exist noticeable differences. As shown in Figure 7, with the increasing number of cycles under the axial pressure of 6.3 MPa and 12.6 MPa, the peak strength of the rock shows a trend of 'strengthening first and then weakening', which was different from the axial pressure of 20.5 MPa and 26.8 MPa. There exists no strength reinforcement at high pre-axial pressure.

The peak stresses of the initial impact under the axial pressure of 12.6 MPa are 42.03 MPa, 51.56 MPa, 49.61 MPa and 47.01 MPa, which are greater than the other three axial pressure conditions. When the number of impacts increases, the magnitude of peak stress degradation in the middle and later stages of this axial compression is more rapid than that of the other three axial compressions. This phenomenon occurs under any pH. This indicates that the dynamic strength of white sandstone at the initial stage is strengthened by 40% axial compression during cyclic impact. However, the axial compression at the middle and later stages will also aggravate the accumulation of internal damage of white sandstone specimens during impact.

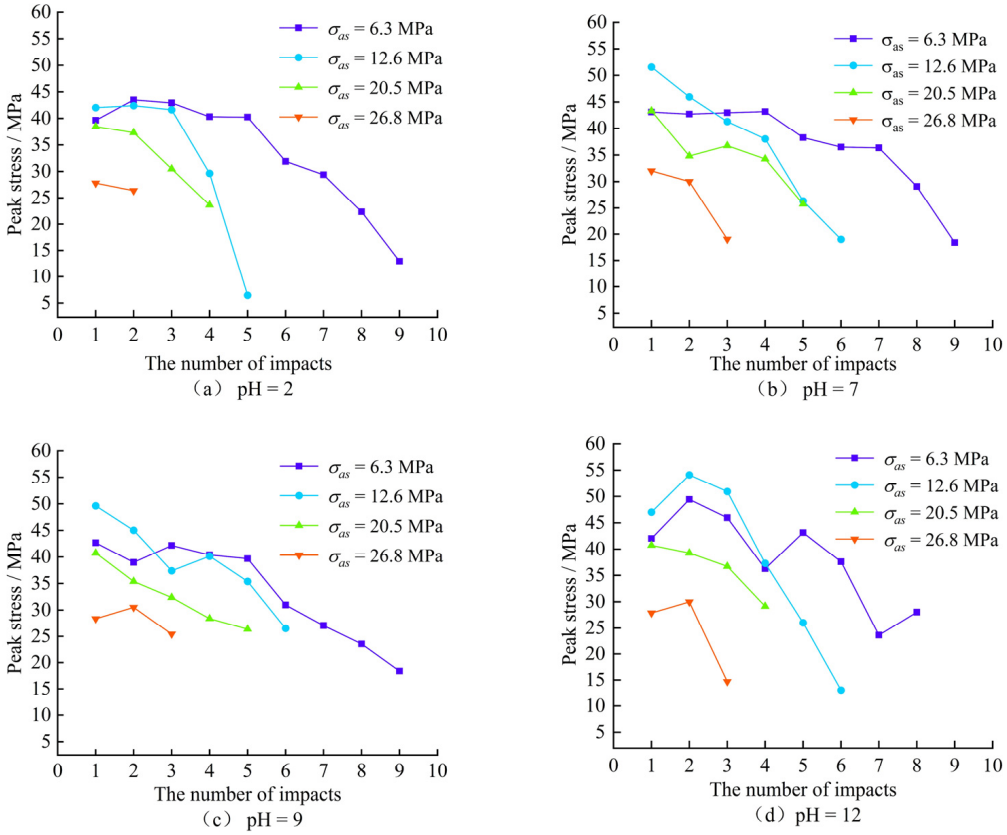

Figure 7. Relationship between peak stress and number of impacts. (**a**) pH = 2; (**b**) pH = 7; (**c**) pH = 9; (**d**) pH = 12.

4.3. Relationship between Peak Stress and Chemical Corrosion

The macroscopic manifestation of the water–rock reaction is the deterioration of the physical and mechanical properties of rock [39]. Figure 8 shows the relationship between the peak stress of the specimen and the chemical solution. Followed by the pH = 12 alkaline solution immersion test piece, the initial impact strength of the specimen is the lowest pH = 2 acid solution immersion. The maximum initial strength of the test piece is in a neutral solution at pH = 7. Complex physical and chemical reactions occur when rocks are immersed in a chemical solution. The physical interaction between water and rock mainly causes sandstone minerals to be dissolved in water. Changes in rock composition and structure are mainly due to the corrosion of minerals in chemical solutions. With the increase of acidity and alkalinity, the damage of rock in solution is mainly determined by chemical reactions. Mineral particles and the ion exchange reaction in the solution generate a new secondary mineral, changing the original mineral chemical composition, the generated secondary mineral composition and molecular weight. Density is very different from the original mineral. Inherent internal cementation way and structure characteristics change accordingly, eventually degrading sandstone in terms of its macro mechanical performance.

In acidic solution, alkaline cations on the surface of feldspar exchange with hydrogen ion in the solution, forming a weak acidic silicon-rich complex. Potassium, sodium, and calcium in feldspar detach from the rock mass skeleton and enter the solution [40].

$$KAlSi_3O_8 + 4H^+ + 4H_2O \rightarrow K^+ + Al^{3+} + 3H_4SiO_4 \quad (4)$$

$$NaAlSi_3O_8 + 4H^+ + 4H_2O \rightarrow Na^+ + Al^{3+} + 3H_4SiO_4 \quad (5)$$

$$CaAl_2Si_2O_8 + 2H^+ + H_2O \rightarrow Ca^{2+} + Al_2Si_2O_5(OH)_4 \quad (6)$$

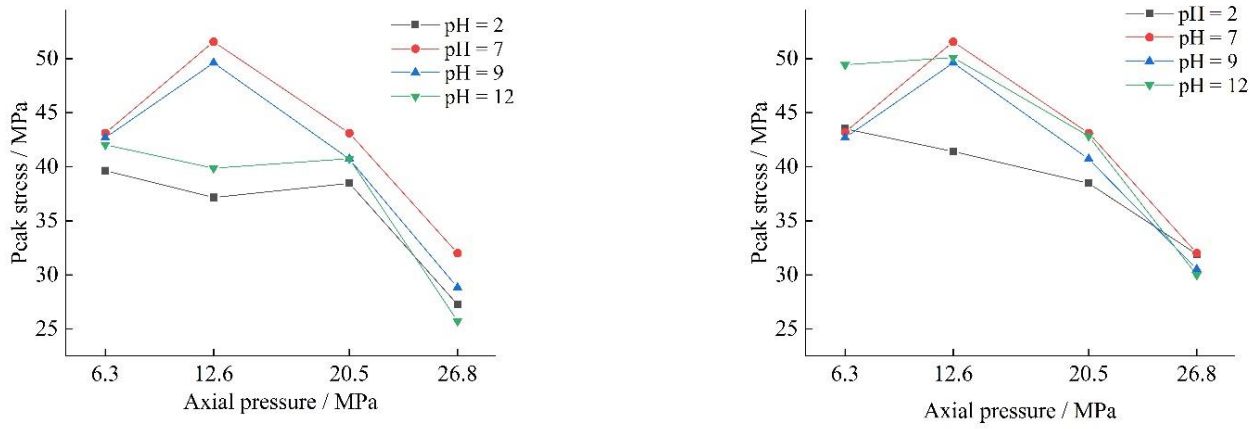

Figure 8. The trend of peak stress. (**a**) initial peak stress; (**b**) the maximum of peak stress.

In addition to the chemical reactions listed earlier, small amounts of hematite, and calcite in the mineral composition of sandstone also react with hydrogen ions in solution.

$$Fe_2O_3 + 6H^+ \rightarrow 2Fe^{3+} + 3H_2O \quad (7)$$

$$CaCO_3 + 2H^+ \rightarrow Ca^{2+} + H_2O + CO_2\uparrow \quad (8)$$

In the neutral solution, the solubility of sandstone components is low. Besides, it is difficult to react violently with the aqueous solution. Only a small amount of feldspar and quicklime participate in the chemical reaction and are stable.

In alkaline solution, hematite, calcite, quicklime, and other minerals in sandstone remain relatively stable. However, quartz and feldspar in sandstone are easy to react with hydroxide ion in alkaline solution.

$$SiO_2 + 2OH^- \rightarrow SiO_3^{2-} + H_2O \quad (9)$$

$$KAlSi_3O_8 + 6OH^- + 2H_2O \rightarrow K^+ + Al(OH)_4^- + 3H_2SiO_4^{2-} \quad (10)$$

$$NaAlSi_3O_8 + 6OH^- + 2H_2O \rightarrow Na^+ + Al(OH)_4^- + 3H_2SiO_4^{2-} \quad (11)$$

The failure mode of white sandstone is shown in Figure 9a–p under cyclic impact. White sandstone specimens mainly experience conjugate hyperbolic tensile shear failure, which was characterized by destructive body flaking around the hyperbola due to interfacial friction. Corrosion by acid and alkaline solutions of sandstone fragments' impact degree is more than with the neutral solution, with a smaller average size of fragments. In an acidic solution, the sandstone is completely disintegrated with a high proportion of fine particle size. Feldspar, clay, hematite, calcite and other minerals in sandstone are captured by solution, resulting in an increase in small particle size fragments. Structural cavities make rock structures become looser and more fragile. In an alkaline solution, the quartz particles on the surface of the specimen will be exfoliated by the solution, thereby increasing the number of fine particles. In neutral solutions, the solubility of mineral components is low, and the degree of fragmentation is mainly dependent on the cyclic shock load.

By testing the broken samples, it has been found that the solution corroded the sandstone and caused the internal cavity of the sandstone to produce structural defects. During cyclic impact, the rock exhibits a low-cycle fatigue damage and strength degradation. Repeated impact causes the rock particles to loosen and fall off. As the number of cycles increases, this phenomenon gradually penetrates into the interior of the sandstone. Meanwhile, the porosity of the internal structure allows the chemical solution to further penetrate into the interior of the sandstone. This interaction improves exposure between chemical solutions and mineral particles, thus allowing for a more thorough chemical

reaction between water and rock. Therefore, the hydration solution and the cyclic shock influence the rate and degree of rock metamorphism while promoting each other in the process of rock metamorphism.

Figure 9. The destructed forms of white sandstone (**a**–**p**).

5. Conclusions

To conclude, this study introduces the cyclic impact test of white sandstone specimens under chemical corrosion and axial compression, as well as stress–strain and dynamic strength variation characteristics. Several vital conclusions are presented as follows:

(1) The stress–strain curve during the cyclic impact test of white sandstone can be divided into three types: an early semi-elliptic high flat curve, a mid-gradient parabola, and low flat parabolic curve.

(2) With the increase of the number of cycles under the same load, the peak strength of the rock shows a trend of 'strengthening first and then weakening'. The strength of stone resistance to impact failure reached its maximum at pH of 7 and axial pressure of 12.6 MPa.

(3) Under the same axial pressure, the effect of solution pH on the initial dynamic strength of white sandstone is a normal distribution. The acidic and alkaline environment damage is harmful to rocks, while neutral environment generates little effect. The

influence of solution pH on the dynamic strength of white sandstone is not apparent during the middle and late periods.

(4) Through carrying out a series of studies, the proper proportion of loading will make the micro-fractures in the white sandstone tend to be tight, and the impact strength of the white sandstone will be strengthened in the early stage. Overloading will aggravate the deterioration of the strength of the white sandstone under the impact and further intensify the damage in the middle and later stages. When the loading ratio exceeds a certain limit, the micro-cracks of the white sandstone will increase due to the increasing loading ratio. Furthermore, the structure of rock will be destroyed.

Author Contributions: Conceptualization, J.X. and L.D.; methodology, J.X.; software, Z.Z.; validation, L.D., Z.Z. and J.J.; formal analysis, Y.Z. (Yingbin Zhang); investigation, Y.Z. (Yihan Zhang); resources, L.T.; data curation, Y.Z. (Yingbin Zhang); writing—original draft preparation, J.X. and Z.Z.; writing—review and editing, J.X. and L.D.; visualization, Z.Z. and R.C.; supervision, L.D.; funding acquisition, J.X. All authors have read and agreed to the published version of the manuscript.

Funding: This research was supported financially by the National Natural Science Foundation of China (No. 51664016, No. 51664017) and the Jiangxi Provincial Department of Education (GJJ150694).

Data Availability Statement: The data used to support the findings of this study are available from the corresponding author upon request.

Conflicts of Interest: The authors declare no conflict of interest.

References

1. Sharifzadeh, M.; Kolivand, F.; Ghorbani, M.; Yasrobid, S. Design of sequential excavation method for large span urban tunnels in soft ground—Niayesh tunnel. *Tunn. Undergr. Space Technol.* **2013**, *35*, 178–188. [CrossRef]
2. Feng, J.; Wang, E.; Shen, R.; Chen, L.; Li, X.; Li, N. A source generation model for near-field seismic impact of coal fractures in stress concentration zones. *J. Geophys. Eng.* **2016**, *13*, 516–525. [CrossRef]
3. Guan, X.; Wang, X.; Zhu, Z.; Zhang, L.; Fu, H. Ground Vibration Test and Dynamic Response of Horseshoe-shaped Pipeline During Tunnel Blasting Excavation in Pebbly Sandy Soil. *Finite Elem. Anal. Des.* **2020**, *38*, 3725–3736. [CrossRef]
4. Dong, L.; Sun, D.; Shu, W.; Li, X. Exploration: Safe and clean mining on Earth and asteroids. *J. Clean. Prod.* **2020**, *257*, 120899. [CrossRef]
5. Bayraktar, A.; Sevim, B.; Altunişik, A.C. Finite element model updating effects on nonlinear seismic response of arch dam–reservoir–foundation systems. *Finite Elem. Anal. Des.* **2011**, *47*, 85–97. [CrossRef]
6. Dong, L.; Deng, S.; Wang, F. Some developments and new insights for environmental sustainability and disaster control of tailings dam. *J. Clean. Prod.* **2020**, *269*, 122270. [CrossRef]
7. Dong, L.-J.; Tang, Z.; Li, X.-B.; Chen, Y.-C.; Xue, J.-C. Discrimination of mining microseismic events and blasts using convolutional neural networks and original waveform. *J. Cent. South Univ.* **2020**, *27*, 3078–3089. [CrossRef]
8. Lu, Z.-D.; Chen, C.-X.; Feng, X.-T.; Zhang, Y.-L. Strength failure and crack coalescence behavior of sandstone containing single pre-cut fissure under coupled stress, fluid flow and changing chemical environment. *J. Cent. South Univ.* **2014**, *21*, 1176–1183. [CrossRef]
9. Li, X.; Li, C.; Cao, W.; Tao, M. Dynamic stress concentration and energy evolution of deep-buried tunnels under blasting loads. *Int. J. Rock Mech. Min. Sci.* **2018**, *104*, 131–146. [CrossRef]
10. Gong, F.Q.; Li, X.B.; Liu, X.L.; Zhao, J. Experimental study of dynamic characteristics of sandstone under one-dimensional coupled static and dynamic loads. *Chin. J. Rock Mech. Eng.* **2010**, *29*, 2076–2085.
11. Zhou, R.; Cheng, H.; Cai, H.; Wang, X.; Guo, L.; Huang, X. Dynamic Characteristics and Damage Constitutive Model of Mudstone under Impact Loading. *Materials* **2022**, *15*, 1128. [CrossRef] [PubMed]
12. Jin, J.F.; Li, X.B.; Wang, G.S.; Yin, Z.Q. Sandstone failure mode and mechanism under cyclic impact load. *J. Cent. South Univ. Nat. Sci. Ed.* **2012**, *43*, 254–262.
13. Ding, W.X.; Feng, X.T. Experimental study on mechanical effects of limestone under chemical corrosion. *J. Rock Mech. Geotech.* **2004**, *23*, 3571.
14. Xie, H.; Li, C.; He, Z.; Li, C.; Lu, Y.; Zhang, R.; Gao, M.; Gao, F. Experimental study on rock mechanical behavior retaining the in situ geological conditions at different depths. *Int. J. Rock Mech. Min. Sci.* **2021**, *138*, 104548. [CrossRef]
15. Siddiqua, S.; Siemens, G.; Blatz, J.; Man, A.; Lim, B.F. Influence of Pore Fluid Chemistry on the Mechanical Properties of Clay-Based Materials. *Geotech. Geol. Eng.* **2014**, *32*, 1029–1042. [CrossRef]
16. Han, T.L.; Shi, J.P.; Chen, Y.S.; Li, Z.H.; Ma, W.T. Experimental study on deterioration of mechanical properties and energy mechanism of calcareous sandstone under water chemistry. *J. Rock Mech. Geotech.* **2015**, *32*, 189–200.

17. Feng, X.-T.; Chen, S.; Li, S. Effects of water chemistry on microcracking and compressive strength of granite. *Int. J. Rock Mech. Min. Sci.* **2001**, *38*, 557–568. [CrossRef]
18. Li, N.; Zhu, Y.M.; Zhang, P.; Ge, X.R. Chemical damage model of calcareous cemented sandstone in acid environment. *Chin. J. Geotech. Eng.* **2003**, *25*, 395–399.
19. Cui, Q.; Feng, X.T.; Xue, Q.; Zhou, H.; Zhang, Z.H. Research on the mechanism of sandstone pore structure change under chemical corrosion. *Chin. J. Rock Mech. Eng.* **2008**, *27*, 134–141.
20. Mokhtarian, H.; Moomivand, H.; Moomivand, H. Effect of infill material of discontinuities on the failure criterion of rock under triaxial compressive stresses. *Theor. Appl. Fract. Mech.* **2020**, *108*, 102652. [CrossRef]
21. Karev, V.I.; Kilmov, D.M.; Kovalenko, Y.F.; Ustinov, K.B. Experimental Study of Rock Creep under True Triaxial Loading. *Mech. Solids* **2019**, *54*, 1151–1156. [CrossRef]
22. Wen, S.; Zhang, C.; Chang, Y.; Hu, P. Dynamic compression characteristics of layered rock mass of significant strength changes in adjacent layers. *J. Rock Mech. Geotech. Eng.* **2019**, *12*, 353–365. [CrossRef]
23. Kumar, J.; Rahaman, O. Lower Bound Limit Analysis Using Power Cone Programming for Solving Stability Problems in Rock Mechanics for Generalized Hoek–Brown Criterion. *Rock Mech. Rock Eng.* **2020**, *53*, 3237–3252. [CrossRef]
24. Yang, W.; Li, G.; Ranjith, P.; Fang, L. An experimental study of mechanical behavior of brittle rock-like specimens with multi-non-persistent joints under uniaxial compression and damage analysis. *Int. J. Damage Mech.* **2019**, *28*, 1490–1522. [CrossRef]
25. Kovrizhnykh, A.M.; Usol'Tseva, O.M.; Kovrizhnykh, S.A.; Tsoi, P.A.; Semenov, V.N. Investigation of Strength of Anisotropic Rocks under Axial Compression and Lateral Pressure. *J. Min. Sci.* **2017**, *53*, 831–836. [CrossRef]
26. Wu, H.; Dai, B.; Cheng, L.; Lu, R.; Zhao, G.; Liang, W. Experimental Study of Dynamic Mechanical Response and Energy Dissipation of Rock Having a Circular Opening Under Impact Loading. *Min. Met. Explor.* **2021**, *38*, 1111–1124. [CrossRef]
27. Zhou, M.; Li, J.; Luo, Z.; Sun, J.; Xu, F.; Jiang, Q.; Deng, H. Impact of water–rock interaction on the pore structures of red-bed soft rock. *Sci. Rep.* **2021**, *11*, 7398. [CrossRef]
28. Bieniawski, Z.T.H. Suggested methods for determining tensile strength of rock materials. *Int. J. Rock Mech. Min. Sci. Géoméch. Abstr.* **1978**, *15*, 99–103. [CrossRef]
29. Li, X.B.; Zhou, Z.L.; Ye, Z.Y.; Ma, C.D.; Zhao, F.J. Research on dynamic and static loading mechanical properties of rock. *J. Rock Mech. Eng.* **2008**, *27*, 96–104.
30. Zi, L.Z.; Xi, B.L.; Ai, H.L.; Yang, Z. Stress uniformity of split Hopkinson pressure bar under half-sine wave loads. *Int. J. Rock Mech. Min.* **2011**, *48*, 697–701. [CrossRef]
31. Zhang, Q.B.; Zhao, J. A Review of Dynamic Experimental Techniques and Mechanical Behaviour of Rock Materials. *Rock Mech. Rock Eng.* **2014**, *47*, 1411–1478. [CrossRef]
32. Cai, M. Practical Estimates of Tensile Strength and Hoek–Brown Strength Parameter m i of Brittle Rocks. *Rock Mech. Rock Eng.* **2010**, *43*, 167–184. [CrossRef]
33. Sun, B.; Ping, Y.; Zhu, Z.; Jiang, Z.; Wu, N. Experimental Study on the Dynamic Mechanical Properties of Large-Diameter Mortar and Concrete Subjected to Cyclic Impact. *Shock Vib.* **2020**, *2020*, 8861197. [CrossRef]
34. Gao, R.; Li, J. Equivalent constant-amplitude fatigue load method based on the energy equivalence principle. *Adv. Struct. Eng.* **2019**, *22*, 2892–2906. [CrossRef]
35. Jin, J.F.; Li, X.B.; Yin, Z.Q. Effects of axial pressure and cyclic impact times on dynamic mechanical properties of sandstone. *J. China Coal Soc.* **2012**, *37*, 923–930.
36. Wang, T.-T.; Shang, B. Three-Wave Mutual-Checking Method for Data Processing of SHPB Experiments of Concrete. *J. Mech.* **2014**, *30*, N5–N10. [CrossRef]
37. Michalowski, R.L.; Park, D. Stability assessment of slopes in rock governed by the Hoek-Brown strength criterion. *Int. J. Rock Mech. Min. Sci.* **2020**, *127*, 104217. [CrossRef]
38. Ma, M.; Brady, B. Analysis of the Dynamic Performance of an Underground Excavation in Jointed Rock under Repeated Seismic Loading. *Geotech. Geol. Eng.* **1999**, *17*, 1–20. [CrossRef]
39. Shang, D.; Zhao, Z.; Dou, Z.; Yang, Q. Shear behaviors of granite fractures immersed in chemical solutions. *Eng. Geol.* **2020**, *279*, 105869. [CrossRef]
40. Han, T.; Li, Z.; Shi, J.; Cao, X. Mechanical characteristics and freeze–thaw damage mechanisms of mode-I cracked sandstone from the Three Gorges Reservoir region under different chemical solutions. *Arab. J. Geosci.* **2021**, *14*, 944. [CrossRef]